JOURNAL OF AIRCRAFT
Vol. 48, No. 2, March–April 2011

Uncertainty Identification of Supersonic Wind-Tunnel Testing

Shinji Nagai* and Hidetoshi Iijima†
Japan Aerospace Exploration Agency, Tokyo 182-8522, Japan

DOI: 10.2514/1.C031159

In this study, a methodology for identification of uncertainty is developed, which have been empirically estimated by multifacility wind-tunnel testing. Instead of this multifacility testing, multiposition testing was performed across a characteristics mesh of supersonic flow. From the variations in aerodynamic coefficients in body axes, the uncertainty caused by flow quality is identified about models of interest. The identified uncertainty is almost dominated by characterization of tunnel flow quality. Then, after consideration of practically independent parameters, uncertainties of aerodynamic coefficients in stability axes are estimated by combining the identified uncertainties in body axes. Their validities are confirmed by correlation results of tunnel-to-tunnel comparison tests.

Nomenclature

Ab	=	model total base area, m^2
Ad	=	distributed base area for each pressure sensor, m^2
Aw	=	reference area, m^2
B	=	bias limit
B'	=	correlated bias limit
c	=	reference chode length, m
CAF	=	forebody axial force coefficient
CDF	=	forebody drag force coefficient
CLF	=	forebody lift force coefficient
CM	=	pitching moment coefficient around balance center
Cm	=	pitching moment coefficient around reference center
CN	=	normal force coefficient
D	=	model diameter, mm
DM	=	delta Mach number determined during wind-tunnel calibration
FA	=	axial force, N
FN	=	normal force, N
g, h, m	=	correction factors
K	=	coverage factor; $K = 2$
L	=	model length; $L = 8.5D$ [mm]
M	=	freestream Mach number
Mp	=	Mach number calculated from the ratio of total pressure $p0$ and pitot pressure pt
Mw	=	wall Mach number calculated from the ratio of total pressure $p0$ and wall pressure pw
My	=	pitching moment, Nm
N	=	number of sample data
P	=	precision limit
$p0$	=	total pressure, Pa
pb	=	base pressure, Pa
$pref$	=	reference pressure for pressure measurement, Pa
ps	=	calculated static pressure, Pa
pt	=	pitot pressure of the test section flow, Pa
pw	=	test section wall pressure, Pa
q	=	dynamic pressure, Pa
ReL	=	Reynolds number based on model length
S	=	standard deviation
U	=	uncertainty
X, Y, Z	=	coordinate, m or variable
α	=	angle of attack, °
θ	=	model pitch angle, °
Φ	=	model roll angle, °

Subscripts

B	=	balance center
C	=	moment reference center
M	=	sensor output such as a balance or a pressure transducer
W	=	model weight

I. Introduction

IT IS required to estimate experimental uncertainty of wind-tunnel testing. In the development of aircraft, flight performances must be predicted from results of wind-tunnel testing and computational fluid dynamics. This uncertainty not only suggests the development risks but also facilitates comparison of data sets among different facilities, computational fluid dynamics, and flight. Additionally, this uncertainty analysis yields the dominant error contributors and aids the collection of outliers of the data. The AIAA published the AIAA-S071A-1999 standard for uncertainty assessment of wind-tunnel testing [1], but assessment of tunnel flow quality remains from as it relies upon experience.

The flow quality is composed of steady and dynamic tunnel flow components and almost dominates the bias error of the wind tunnel. Traditionally, the bias error of a wind tunnel has been empirically estimated from the correlation results of time-consuming multifacility wind-tunnel testing [2–4]. After the AIAA standard was issued, uncertainty analyses were carried out for typical tests performed in many wind tunnels [5,6]. It was found that the major contributors to the uncertainty of wind-tunnel data are calibration of wind-tunnel flow and strain gage balances [7,8]. Further, It was found that in supersonic flow, nonuniformity of the freestream Mach number is the dominant contributor to uncertainty [9,10]. Because the error contribution of the abovementioned flow quality depends on the configuration of the test model, no methodology has yet been established for estimating the uncertainty of wind-tunnel testing for any models of interest.

According to the AIAA standard, the root-sum-square of all products of each error of a measured variable and its partial derivative are calculated. The standard recommends that this partial derivative of the result should be taken with respect to the measured variable, because the measured variables are principally independent parameters. These complex procedures are recommended to be calculated by dedicated software in a facility. However, small error contributors could often be negligible in this root-sum-square calculation. Thus, it might be possible not only to ignore them but also to reorganize them as practically independent parameters from an aerodynamic

Presented as Paper 2010-0743 at the 48th AIAA Aerospace Sciences Meeting, Orlando, 4–7 January 2010; received 23 June 2010; revision received 24 September 2010; accepted for publication 24 September 2010.

*Senior Researcher, Aerospace Research Directorate, 7-44-1 Jindaijihigashi-machi, Chofu. Senior Member AIAA.

†Researcher, Aerospace Research Directorate, 7-44-1 Jindaijihigashi-machi, Chofu. Member AIAA.

viewpoint, even if they cannot be considered as independent parameters from a mathematical viewpoint.

In this paper, a methodology for uncertainty identification of supersonic wind-tunnel testing is proposed. First, an initial uncertainty analysis is carried out for aerodynamic coefficients of an AGARD-B calibration model [11]. Then, three kinds of multiposition tests are performed in one wind tunnel to assess error contributions of the flow quality for any models of interest. Next, with these results, our uncertainty identification methodology and practically independent parameters are discussed. Finally, the identified uncertainties are combined for being validated by correlation results of tunnel-to-tunnel comparison tests.

II. Wind-Tunnel Testing for Uncertainty Assessment

A. Wind-Tunnel Models and a Test Section

A schematic figure of the AGARD-B calibration model is shown in Fig. 1. Two models with reference diameters of 0.045 and 0.075 m were used in this study. These models are hereafter referred to as the $D = 45$ and $D = 75$ models, respectively. Aerodynamic coefficients of the both model were obtained in the Japan Aerospace Exploration Agency (JAXA) 1 m × 1 m supersonic wind tunnel (JSWT). The boundary-layer transitions on the wings and the bodies of the both models were fixed at the common location [11] with minimum height roughness.

Figure 2 shows the JSWT test section installed of $D = 75$ model and definitions of coordinate, aerodynamic forces and moment. The solid wall type test section is 1 m × 1 m in the cross section and 1.8 m long. The model support gives model attitude in 3 degrees of freedom, pitch angle θ, roll angle ϕ, and height, in other words, coordinate Z. Three pressure ports were located at 0.64 m upstream from the center of the side window and $Z = 0, \pm 0.2$ m. On the other side wall, there are another three pressure ports at the same location. These six ports are connected each other and wall pressure Pw of the wind tunnel was measured.

B. Tunnel Flow Calibration

The tunnel flow of the JSWT was calibrated by a pitot rake and an example of the results is shown in Fig. 3. The vertically two-dimensional (2-D) symmetric nozzle consists of flexible upper and lower plates; the flow was sufficiently 2D to be calibrated in the vertical center plane. Mach number distributions were obtained using

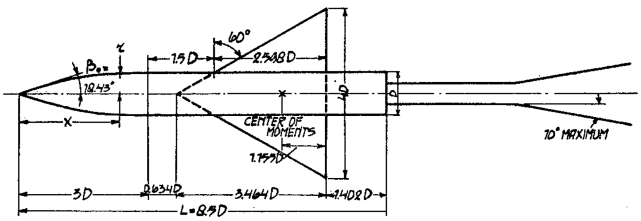

Fig. 1 A planform of the AGARD-B calibration model.

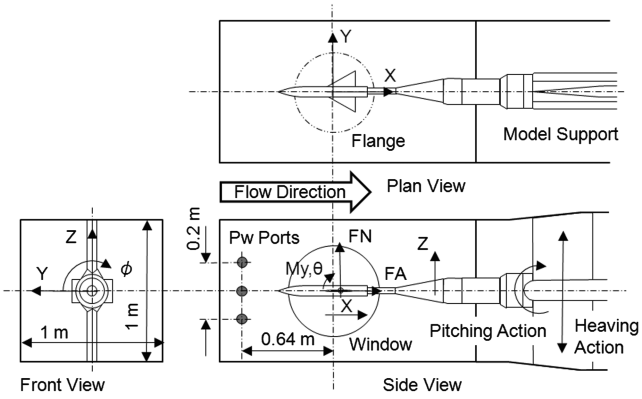

Fig. 2 Test section installed of $D = 75$ AGARD-B model.

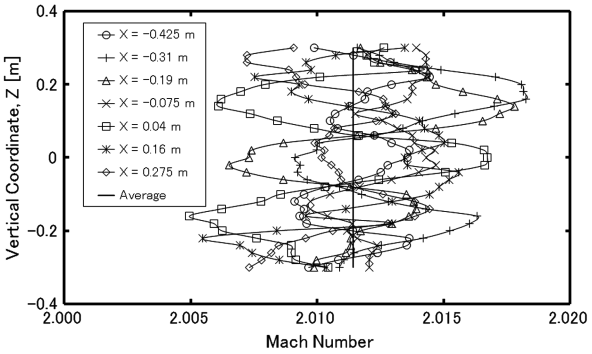

Fig. 3 Mach number distributions at a nozzle Mach number of 2.

a vertical pitot rake with a 20 mm pitch at seven stations located 0.425 m upstream to 0.275 m downstream of the side window center in the test section. In the range of the vertical coordinate of ±0.3 m, 31 point pitot pressures were obtained at one streamwise station. Seven tests were carried out to obtain the vertical pitot pressure distributions at the seven streamwise stations. Mach numbers are calculated from the ratios of common total pressure $p0$ and each pitot pressure pt. An averaged Mach number was 2.012 in the uniform core of ±0.3 m in the vertical coordinate. The Mach number deviations from the averaged value are quite small as less than 0.5% because the nozzle aerolines were optimized by using computational fluid dynamics technologies [12]. By the nature of supersonic flow, disturbances caused by the pitot rake only propagate downstream within the Mach angle. Thus the flow uniformity can be assessed by such pitot pressure measurements.

From these data, the delta Mach number DM was previously determined as the difference between the averaged Mach number and a wall Mach number Mw calculated from the ratio of $p0$ to pw as shown below. Mw_j is the wall Mach number during the calibration test of the jth streamwise station

$$DM = \sum_{j=1}^{7} \frac{\sum_{i=1}^{31} \frac{Mp_{i,j}}{31}}{7} - \sum_{j=1}^{7} \frac{Mw_j}{7} \tag{1}$$

$$Mw = \left(5\left[\left(\frac{p0}{pw}\right)^{\frac{2}{7}} - 1\right]\right)^{\frac{1}{2}} \tag{2}$$

where $Mp_{i,j}$ is the Mach number at the ith vertical point in the jth streamwise station and it satisfies the normal shock relationship as shown in the equation below [13].

$$\frac{pt_{i,j}}{p0} = \left(\frac{6Mp_{i,j}^2}{Mp_{i,j}^2 + 5}\right)^{\frac{7}{2}} \left(\frac{6}{7Mp_{i,j}^2 - 1}\right)^{\frac{5}{2}} \tag{3}$$

The wall Mach numbers among the seven station tests showed good repeatability less than the estimated precision limit of Mw as mentioned in the following section. The values of DM were stored and expressed as a function of averaged wall Mach number of the seven tests. In the usual test, the wall Mach number Mw was calculated again from the measured values of $p0$ and pw during the test. Then, the delta Mach number DM correspondent to the Mw during the test was added to obtain the freestream Mach number as following equations. This freestream Mach number was then used to calculate the freestream dynamic and static pressures

$$M = Mw_{\text{test}} + DM \tag{4}$$

C. Initial Uncertainty Analysis

An initial uncertainty analysis was carried out for the test of the $D = 75$ AGARD-B model. The uncertainty interval U about the measured value of X is the band within which the experimenter is 95% confident the true value of the variable lies [14]. The uncertainty

U is consisted of a bias limit B and a precision limit P. The 95% confidence uncertainty is given by

$$U = \pm(B^2 + P^2)^{\frac{1}{2}} \tag{5}$$

The precision limit P for a measured variable X is given by

$$P = \pm K \cdot S \tag{6}$$

where K is the coverage factor and equals two for a 95% confident level, S is the standard deviation of the sample N readings of the variable X and is defined as

$$S = \sqrt{\frac{\sum_{i=1}^{N}(X_i - \frac{1}{N}\sum_{j=1}^{N} X_j)^2}{(N-1)}} \tag{7}$$

The bias limit B is estimated with the understanding that the experimenter is 95% confident that the true value of the bias error, if known, would be less than the interval B. The information of specifications, analytical estimates, and previous experience will typically provide the basis for most of the estimates. These estimates can be updated using the additional information gained about the errors associated with calibration process, for example.

The precision limit and the bias limit of the experimental result computed using the measured variables in data reduction equations are calculated as follows. The precision limit of the result is combined with precision limits of measured variables and constants principally because they are independent parameters. The bias limit of the result is also calculated in the same way but correlated bias errors are taken into account. For example, the forebody axial force coefficient is a function of the measured values of total pressure $p0$, test section wall pressure pw, delta Mach number DM, balance axial force FA_M, model weight correction FA_W, base pressure pb and reference pressure $pref$. The root-sum-square of all products of each limit and its partial derivative is calculated.

Further, the uncertainties of model weight corrections were assessed by end-to-end evaluation with no-wind data. The result of this end-to-end evaluation showed us that these uncertainties were sufficiently small compared with the uncertainties of the measured force and moment. Thus, constant uncertainties in the whole range of model attitude angles were adopted, and then, the uncertainties of pitch and roll angles of the model were eliminated in the following equations [15]. The base pressures were measured with four independent pressure sensors but they are calibrated by a common working standard. The model support interference and wall interference are ignored by the nature of supersonic flow. There are no correction terms for them

$$CAF = \frac{FA - (ps - pb)\cdot Ab}{q \cdot Aw} \tag{8}$$

$$pb = \sum_{i=1}^{4} \frac{Ad_i}{Ab} pb_{M_i} \tag{9}$$

$$Ab = \sum_{i=1}^{4} Ad_i \tag{10}$$

$$B_{CAF} = \pm\left(\left[\frac{\partial CAF}{\partial p0}B_{p0}\right]^2 + \left[\frac{\partial CAF}{\partial pw}B_{pw}\right]^2 + \left[\frac{\partial CAF}{\partial DM}B_{DM}\right]^2 + \left[\frac{\partial CAF}{\partial FA_M}B_{FA_M}\right]^2 + \left[\frac{\partial CAF}{\partial FA_W}B_{FA_W}\right]^2 + \sum_{i=1}^{4}\left[\frac{\partial CAF}{\partial pb_{M_i}}B_{pb_{M_i}}\right]^2 + \left[\frac{\partial CAF}{\partial pref}B_{pref}\right]^2 2\frac{\partial CAF}{\partial p0}\frac{\partial CAF}{\partial pw}B'_{p0}B'_{pw} + 2\sum_{i(j}^{4}\frac{\partial CAF}{\partial pb_{M_i}}B'_{pb_{M_i}} \cdot \frac{\partial CAF}{\partial pb_{M_j}}B'_{pb_{M_j}} + 2\frac{\partial CAF}{\partial FA_M}\frac{\partial CAF}{\partial FA_W}B'_{FA_M}B'_{FA_W}\right)^{\frac{1}{2}} \tag{11}$$

$$P_{CAF} = \pm\left(\left[\frac{\partial CAF}{\partial p0}P_{p0}\right]^2 + \left[\frac{\partial CAF}{\partial pw}P_{pw}\right]^2 + \left[\frac{\partial CAF}{\partial DM}P_{DM}\right]^2 + \left[\frac{\partial CAF}{\partial FA_M}P_{FA_M}\right]^2 + \left[\frac{\partial CAF}{\partial FA_W}P_{FA_W}\right]^2 + \sum_{i=1}^{4}\left[\frac{\partial CAF}{\partial pb_{M_i}}P_{pb_{M_i}}\right]^2 + \left[\frac{\partial CAF}{\partial pref}P_{pref}\right]^2\right)^{\frac{1}{2}} \tag{12}$$

$$U_{CAF} = \pm(B_{CAF}^2 + P_{CAF}^2)^{\frac{1}{2}} \tag{13}$$

$$CN = \frac{FN}{q \cdot Aw} \tag{14}$$

$$B_{CN} = \pm\left(\left[\frac{\partial CN}{\partial p0}B_{p0}\right]^2 + \left[\frac{\partial CN}{\partial pw}B_{pw}\right]^2 + \left[\frac{\partial CN}{\partial DM}B_{DM}\right]^2 + \left[\frac{\partial CN}{\partial FN_M}B_{FN_M}\right]^2 + \left[\frac{\partial CN}{\partial FN_W}B_{FN_W}\right]^2 + 2\frac{\partial CN}{\partial p0}\frac{\partial CN}{\partial pw}B'_{p0}B'_{pw} + 2\frac{\partial CN}{\partial FN_M}\frac{\partial CN}{\partial FN_W}B'_{FN_M}B'_{FN_W}\right)^{\frac{1}{2}} \tag{15}$$

$$P_{CN} = \pm\left(\left[\frac{\partial CN}{\partial p0}P_{p0}\right]^2 + \left[\frac{\partial CN}{\partial pw}P_{pw}\right]^2 + \left[\frac{\partial CN}{\partial DM}P_{DM}\right]^2 + \left[\frac{\partial CN}{\partial FN_M}P_{FN_M}\right]^2 + \left[\frac{\partial CN}{\partial FN_W}P_{FN_W}\right]^2\right)^{\frac{1}{2}} \tag{16}$$

$$U_{CN} = \pm(B_{CN}^2 + P_{CN}^2)^{\frac{1}{2}} \tag{17}$$

$$CM = \frac{My}{q \cdot Aw \cdot c} \tag{18}$$

$$B_{CM} = \pm\left(\left[\frac{\partial CM}{\partial p0}B_{p0}\right]^2 + \left[\frac{\partial CM}{\partial pw}B_{pw}\right]^2 + \left[\frac{\partial CM}{\partial DM}B_{DM}\right]^2 + \left[\frac{\partial CM}{\partial My_M}B_{My_M}\right]^2 + \left[\frac{\partial CM}{\partial My_W}B_{My_W}\right]^2 + 2\frac{\partial CM}{\partial p0}\frac{\partial CM}{\partial pw}B'_{p0}B'_{pw} + 2\frac{\partial CM}{\partial My_M}\frac{\partial CM}{\partial My_W}B'_{My_M}B'_{My_W}\right)^{\frac{1}{2}} \tag{19}$$

$$P_{CM} = \pm\left(\left[\frac{\partial CM}{\partial p0}P_{p0}\right]^2 + \left[\frac{\partial CM}{\partial pw}P_{pw}\right]^2 + \left[\frac{\partial CM}{\partial DM}P_{DM}\right]^2 + \left[\frac{\partial CM}{\partial My_M}P_{My_M}\right]^2 + \left[\frac{\partial CM}{\partial My_W}P_{My_W}\right]^2\right)^{\frac{1}{2}} \tag{20}$$

$$U_{CM} = \pm(B_{CM}^2 + P_{CM}^2)^{\frac{1}{2}} \tag{21}$$

The uncertainty budget for the forebody axial force coefficient CAF at a Mach number of 2.0 and an angle of attack of 4° is shown in Fig. 4. The uncertainties of four base pressures were combined according to Eq. (9) just for an illustration of the small contribution of pb in this figure. The uncertainty of the delta Mach number DM dominates the uncertainty of CAF.

The uncertainty of the delta Mach number DM is estimated as follows. Initially, the 95% precision limit was calculated as 0.006 from the data as shown in Fig. 3. This statistically assessed value was temporally used as a bias limit of DM. This is because the aerodynamic coefficient error resulting from aerodynamic phenomena

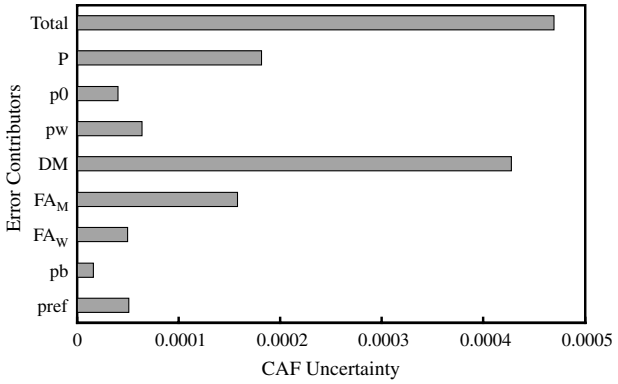

Fig. 4 Uncertainty budget for forebody axial force coefficient CAF.

cannot be directly explained by such a random distribution of Mach number. However, this initial analysis showed us that the stream nonuniformity dominates the uncertainty of conventional test results.

D. Traditional Multifacility Wind-Tunnel Testing

The abovementioned nonuniformity is a major component of flow quality. The flow quality is an inherent characteristic of each wind tunnel and it is a part of tunnel bias error. The tunnel bias error is traditionally estimated from data scatters in multifacility wind-tunnel testing. These data of the model with the common configuration should be obtained at the same test conditions such as the same Mach number and Reynolds number.

Moreover, some requirements should be satisfied before a wind-tunnel experiment can be considered [16]. For example, all the instruments should be traced back to the national standard. Additionally, the freestream conditions should be determined after the uniformity assessment of the flow as shown in the previous section. In such supersonic wind tunnels, the uncertainties are dominated by the flow quality errors as shown in Fig. 4. Although the standard models have simple configurations, much attention should be paid to the model fidelity and testing procedure. Thus one model is often tested in different wind tunnels, even by the same testing personnel.

Here, the aerodynamic characteristics with the fixed transition are principally discussed since they are most important to predict flight performances. For industrial purposes, appropriate boundary-layer trips are usually used to compensate low Reynolds number of the scaled wind-tunnel model. In multifacility wind-tunnel testing, the same boundary-layer trips are often used to minimize the effects of flow disturbance and trip drag. Although the former one largely depends on effectiveness of a settling chamber of each wind tunnel, the transition can be fixed in a controlled manner.

If these requirements are satisfied, the data of the same model configuration scatter mainly because each wind tunnel has each error contribution of flow quality. This error contribution appears a small or large, in other words, random data scatter of the aerodynamic coefficient. If we had plenty data of more than 10 wind tunnels, the uncertainty could be assessed by a statistical procedure [17]. However, the error contribution of flow quality also depends on the model configuration and usually number of the data is limited to a few or little more. Thus, engineering judgment is required to estimate the uncertainty from the data scatter by a few wind tunnels [4,18].

III. Identification Methodology

A. Scope of the Methodology

This methodology yields us the data uncertainty dominated by the flow quality error of the wind tunnel, in which the multiposition tests were conducted with the model of interest. Here, the multiposition tests described later were conducted in the JSWT and the uncertainties of the JSWT data are identified. It is not necessary that all the data obtained in multifacility wind-tunnel testing fall within the JSWT uncertainty intervals around the JSWT data. However, each uncertainty interval of each wind tunnel should have the overlapping potion each other, because the true value ideally lies in this overlapping potion of all the uncertainties around each data value [19].

Again, there has been no information of the tunnel bias error without multifacility wind-tunnel testing so far. Even in multifacility wind-tunnel testing, wind tunnels with poor flow qualities would give us the wider data scatters. Thus the erroneous averaged data value and the wider uncertainty interval would be estimated. If we identify each uncertainty of each wind tunnel by this methodology, it gives us not only useful information for engineering judgment but also the data value closer to the true value by weighted averaging with the uncertainty intervals. The overall uncertainty is also calculated more accurately by this weighted averaging procedure [19].

In this paper, the uncertainties of longitudinal forces and moment about the AGARD-B models are examined because the AGARD-B model has a symmetric configuration without tail wings. However, this methodology can be also applied to identify the uncertainties of the lateral force and moment data. Because the AGARD-B model has a small delta wing with low aspect ratio, the aeroelastic deformation effect is ignored.

These assumptions make up the scope for the following discussions.

B. Flow Structure and Possible Error

In many supersonic wind tunnels, vertically 2-D variable nozzles are employed. The structure of the supersonic nozzle flow is determined by a characteristics mesh [20] as shown in Fig. 5. The flow is accelerated by expansion waves from the nozzle walls in the expansion section; these expansion waves are canceled by compression waves from the nozzle walls in the downstream straightening section. However, numerous weak compression and expansion waves remain even after the cancellation, and local flow properties vary according to these waves as shown in Fig. 5. Across the wave, the local streamline bends and the local Mach number, static pressure and dynamic pressure vary [20]. In reality, numerous weak waves superpositioned linearly and became a wave fan and small stepwise variations became a broader gradient variation as shown in Fig. 3.

If a model is placed on the center line as shown in Fig. 6, each part of the model is exposed to a Mach number, dynamic pressure, and static pressure whose values are different from those calculated from the freestream Mach number. Furthermore, not only the local flow properties but also aerodynamic phenomena are affected by the remaining waves. Although the model itself generates pressure and shock waves in the flowfield, these wave effects are linearly superpositioned on the flowfield [12] and then abbreviated in the figure. In addition, the model blocks the waves across the center line near its surface. Thus, such nonuniformities inevitably result in test errors in supersonic wind-tunnel testing.

Typical transonic wind tunnels have the same supersonic flow structure even in the slotted or perforated wall test sections. In this case, the flow is accelerated to supersonic speed partly by bleeding the air, but numerous 3-D weak pressure waves are generated by the slots, porosities and the bleeding air. Because of its relatively low supersonic speed, these waves easily propagate to the model position and the local flow properties vary in the same manner but in more complex 3D. In this paper, the 2-D characteristics mesh flow in the solid wall test section of the typical supersonic wind tunnel is

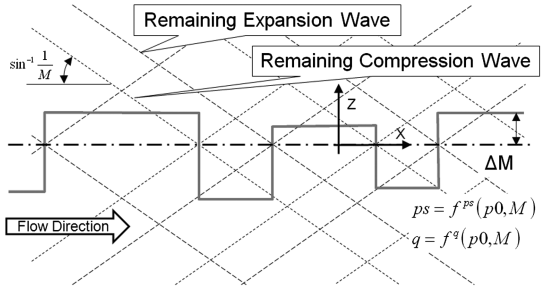

Fig. 5 Flow structure of supersonic wind tunnel.

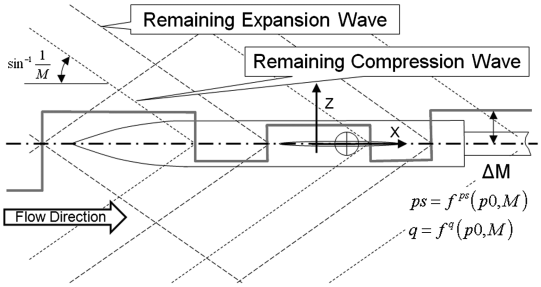

Fig. 6 Inevitable error of local flow properties.

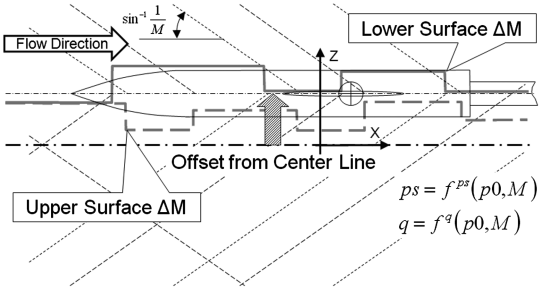

Fig. 8 Vertical position test.

discussed because of its simple structure. However, the methodology can be applied in the typical transonic wind tunnels, if the flowfield around the model is mostly supersonic.

C. Concepts of Multiposition Test

To assess the error contributions of flow quality, three kinds of multiposition tests were performed. The data variations in these multiposition tests were considered to be the equivalents of the data variations in multifacility wind-tunnel testing.

First, a streamwise position test was performed as shown in Fig. 7. The $D = 45$ (smaller) model, whose length was 383 mm, was used to measure the data differences across the calibrated flow space in the flow direction. This model was anticipated to be exposed to all the possible flow nonuniformities at four streamwise positions: upstream, center, downstream, and downstream center positions. However, it is necessary to use a model smaller than a typical model to change the streamwise position in the calibrated space.

Second, a vertical position test was performed as shown in Fig. 8. If a model is made to traverse vertically in the test section, the model is anticipated to be possibly exposed to various combinations of pressure waves propagating along a Mach angle. The model also experience some pressure waves in its upstream and downstream positions. However, even in the 2-D symmetric nozzle, the upper surface of the model is exposed to the local flow properties that are different from those experienced by its lower one, because the pressure waves become asymmetric at the offset position from the center line of the nozzle. Such asymmetric local flow properties might result in an excessively large error of longitudinal aerodynamic force and moment.

D. Results of Axial Force Obtained in Vertical Position Tests

Vertical position tests were performed for the two different-sized models, the $D = 45$ and $D = 75$ models, with various roll angles. The axial force coefficients measured in these tests are shown in Fig. 9. In this figure, variations in the forebody axial force coefficient with the vertical coordinate are plotted and the error bar shows the estimated precision limit. The two-headed arrow shows the initially estimated uncertainty.

The axial force coefficients of both models vary with a change in the vertical position, even if the angle of attack is maintained at a constant value of 0°. The two models show two different results because of the difference in their Reynolds numbers [11]. Even when the roll angle is changed, almost the same variation is observed, but the variation intervals in these cases depend on the model size. The larger model shows smaller variations. Further, the variation intervals are not affected by the angle of attack as shown later.

The ranges of these variations were larger than the estimated precision limit of ±0.0002, but comparable to the estimated uncertainty of ±0.0004. The freestream Mach number error contributes to not only the dynamic pressure error but also the static pressure error in the base pressure correction. The static pressure in the area of the model base varies as shown in Fig. 8. As vertical position changes, the local flow properties are varied by other pressure waves. Although the actual base pressure deviates from the representative static pressure because of the sting interference [11], this deviation is assumed to be superpositioned on the static pressure under the effect of the stream nonuniformities. On the other hand, the dynamic pressure on the model is anticipated to be averaged to the freestream dynamic pressure on the entire model surface.

E. Results of Normal Force and Pitching Moment Obtained in Vertical Position Tests

The normal force and pitching moment coefficients obtained in the vertical position tests are shown in Figs. 10 and 11, respectively. Variations in these coefficients with the vertical coordinate are plotted and the error bars show the estimated precision limits. The two-headed arrows show the initially estimated uncertainty for an angle of attack of 0°.

Although this angle of attack is maintained at 0°, large variations in the normal force and pitching moment are observed with a change in the vertical position. Moreover, these variations depend on the roll angles of the model. The variation ranges decrease as the roll angle approaches 90°.

These variation ranges are considerably larger than the estimated uncertainty intervals based on the statistical assessment of the steam nonuniformities, as discussed in the previous section. As shown in Fig. 8, the local flow properties differ between the upper and lower

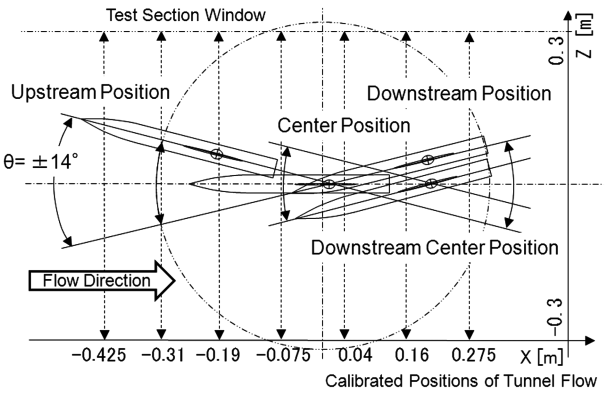

Fig. 7 Streamwise position test.

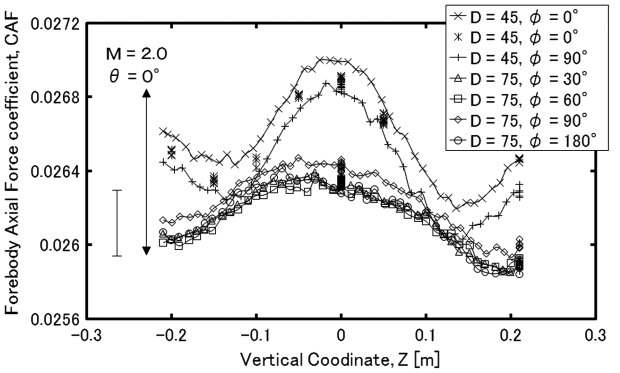

Fig. 9 Variations of axial force coefficients obtained in vertical position tests.

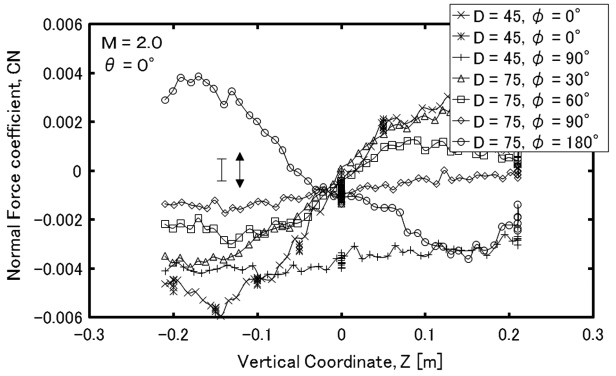

Fig. 10 Variations of normal force coefficients obtained in vertical position tests.

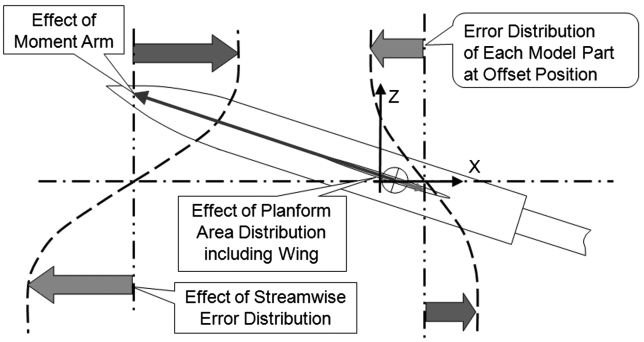

Fig. 12 Offset error effects on longitudinal force and moment of the model.

sides of each part of the model by the asymmetric different pressure waves. It causes larger variations for the equivalents of multifacility wind-tunnel testing because the model are usually located near the center line of the test section.

The above mentioned results show that the three load components, axial force, normal force, and pitching moment, have quite different tendencies of variation with the vertical position. Consequently, the error contributions of the stream nonuniformities are sufficiently independent of each other.

F. Reference Vertical Range and Rotation Center Tests

It is necessary to consider a reference vertical range so that the equivalent variations can be obtained about the normal force and pitching moment.

The error distributions at the offset position are indicated by dashed lines in Fig. 12. Each model part that is offset from the center line is assumed to have error distributions as shown by these dashed lines. A larger error occurs at the vertical position that is farther from the center line. This offset error is also assumed to vary its amount and direction with the streamwise position, as shown in Fig. 12. It is because the asymmetric combinations of the pressure waves are supposed to be changed according to the streamwise position.

Then, this erroneous aerodynamic force of each model part sums up to the erroneous normal force and pitching moment. The model part that has a large wing area or a long moment arm extending toward the reference center contributes significantly to the force and moment errors. The best model position is considered to be the position that minimizes the area of the model part offset from the center line. However, it cannot be ensured that the true value is obtained at this position because of the streamwise distributions of the offset error, model area and moment arm. At least, it is necessary to estimate this total offset error with the model of interest, itself.

A conservative estimate of the uncertainty can be obtained even though the true value is unknown. A reference vertical range is then determined as the range in which a model part located between the nose and the aft end remains on the center line, i.e., the symmetric plane of the 2-D nozzle at a given angle of attack. In the typical test, at least one model part is assumed to remain on the center line and be exposed to the limited extent of the offset errors caused by the asymmetric wave combinations.

A large volume of experimental data needs to be obtained to assess the data statistically. We also conducted this vertical position test in a certain range of angle of attack by changing the rotation center of the pitching action. Here, we set four rotation centers as shown by the closed circles in Fig. 13. Then, we obtained the large number of sample data for angles of attack from −10 to 10° with roll angles of 0 or 180°. This is a series of rotation center tests, the third uncertainty assessment test we performed.

To predict flight performances, it is necessary to obtain the aerodynamic data in some range of side slip angle and angle of attack. In many high speed wind tunnels, side slip angle of the model is accomplished by combination of the model roll and pitch angle because the drag of the model support system have to be minimized as shown in Fig. 2. Accordingly, nonzero angles of attack with side slip angle of 0° can be accomplished only at roll angles of 0 or 180°. Fortunately, the largest normal force and pitching moment error were observed at the roll angles of 0 and 180° as shown in Figs. 10 and 11.

G. Assessment of Flow Quality Errors

The above mentioned variations might be noticed by careful experimentalists, but there has not been any assessment methodologies of these variations in consistent with the uncertainty analysis. An example of longitudinal force and moment data obtained at a Mach number of 2.0 is shown in Fig. 14. As can be observed from the figure, the normal force and pitching moment coefficients (*CN* and *CM*, respectively) are dependent on the angle of attack. Our assessment methodology is illustrated in this magnified graph around an angle of attack of 4°.

Mostly, eight data values were obtained at a single value of the angle of attack, because there were four rotation centers or streamwise positions and two roll angles of 0 or 180°, that is, upright and inverted model positions. These eight data values include all possible

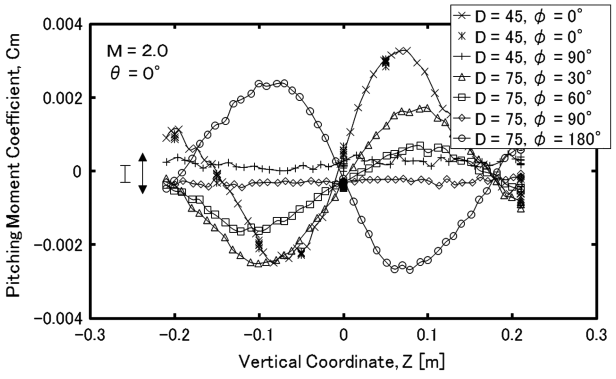

Fig. 11 Variations of pitching moment coefficients obtained in vertical position tests.

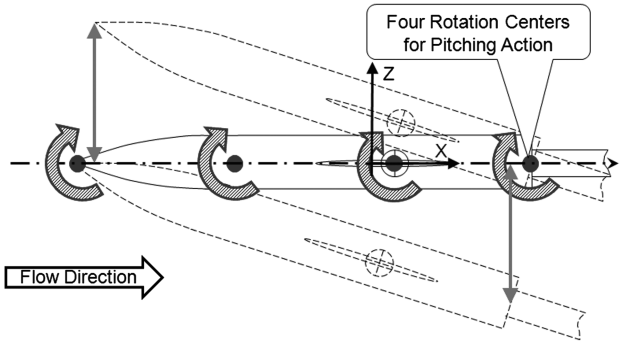

Fig. 13 Rotation center changing test.

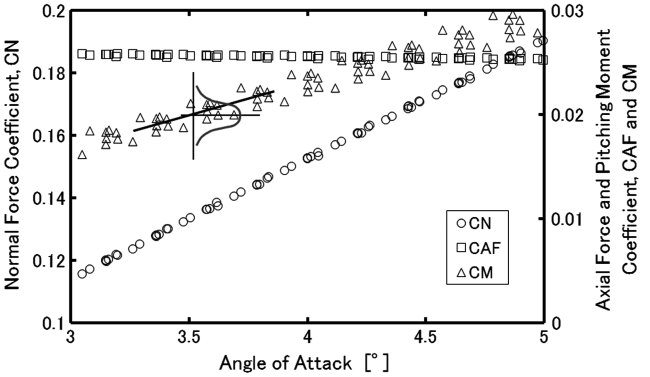

Fig. 14 Data around angle of attack of 4°.

errors caused not only by the stream nonuniformities but also by the dynamic component of the flow quality such as flow unsteadiness.

The flow angularity in the wind-tunnel test section depends on both the flowfield and the model characteristics [21]. The flow angularities about our two models were obtained from the results of normal force measured in the tests at these upright and inverted positions around an angle of attack of 0°; this flow angularity of each model corrected all angles of attack of each model. Between the upright and inverted positions, the model nose was located upper or lower side to the center line of the 2-D nozzle. It is still anticipated that the results of these upright and inverted position tests contain errors caused by asymmetric characteristics of the flow. This error is often caused by the flange bumps of the test section wall.

A simple linear regression model [22] was used to assess the data in limited ranges of the angle of attack. The 24 data values were used to calculate the standard error of estimation (SEE) [19] at a particular angle of attack. These data correspond to those at angles of attack in the range of ±0.2°. We assumed that the aerodynamic coefficients are linear functions of the angle of attack in this limited range. Then, SEE and the assessed uncertainty U_{assessed} were calculated as follows for the streamwise position test and the rotation center test.

$$\text{SEE} = \sqrt{\frac{\sum_{i=1}^{N}(Y_i - Y_{\text{Least Square},i})^2}{(N-2)}} \tag{22}$$

$$U_{\text{assessed by Rotation Center Test or Streamwise Position Test}} = \pm K \cdot \text{SEE} \tag{23}$$

where N is the number of the data and equals 24. The angle of attack itself has an uncertainty of ±0.02°, which corresponds to a normal force coefficient CN error of 0.00075 and pitching moment coefficient CM error of 0.00025. For further discussion, it is necessary to ensure that the assessed uncertainty is sufficiently larger than the uncertainty caused by the uncertainty of angle of attack. The uncertainty of angle of attack included the uncertainty of flow angularity measurement.

Because the angle of attack was maintained constant in the vertical position tests, the standard deviation S of all the data were calculated instead of SEE for the vertical position test

$$U_{\text{assessed by Vertical Position Test}} = \pm K \cdot S \tag{24}$$

H. Identification of Uncertainties by Correction Factors

If the assessed uncertainties are larger than the estimated uncertainties, the correction factors g, k, and m are identified as shown in the following equations. These correction factors physically relate to the actual error contribution of the flow quality of the wind tunnel to the aerodynamic data of the model of interest, with which the multiposition tests were conducted. As seen in the equations below, only three variables are included as the flow parameters, $p0$, pw, and DM. Total pressure $p0$ is kept constant in the supersonic characteristics mesh flow, and wall pressure pw is not appropriate to express the nonuniformities in the supersonic core flow. By contrast, the value of DM was calculated from the average value of the various Mach numbers in the core flow as shown in Fig. 3. Therefore, DM is the only parameter that can reflect the stream nonuniformities that is considered as a bias error. For simplicity, such constant correction factors for various angles of attack were employed in this study

$$\begin{aligned} B_{CAF,\text{identified}} = \pm\Bigg(&\left[\frac{\partial CAF}{\partial p0}B_{p0}\right]^2 + \left[\frac{\partial CAF}{\partial pw}B_{pw}\right]^2 \\ &+ \left[\frac{\partial CAF}{\partial DM}(g\cdot B_{DM})\right]^2 + \left[\frac{\partial CAF}{\partial FA_M}B_{FA_M}\right]^2 + \left[\frac{\partial CAF}{\partial FA_W}B_{FA_W}\right]^2 \\ &+ \sum_{i=1}^{4}\left[\frac{\partial CAF}{\partial pb_{M_i}}B_{pb_{M_i}}\right]^2 + \left[\frac{\partial CAF}{\partial pref}B_{pref}\right]^2 + 2\frac{\partial CAF}{\partial p0}\frac{\partial CAF}{\partial pw}B'_{p0}B'_{pw} \\ &+ 2\sum_{i<j}^{4}\frac{\partial CAF}{\partial pb_{M_i}}B'_{pb_{M_i}}\cdot\frac{\partial CAF}{\partial pb_{M_j}}B'_{pb_{M_j}} + 2\frac{\partial CAF}{\partial FA_M}\frac{\partial CAF}{\partial FA_W}B'_{FA_M}B'_{FA_W}\Bigg)^{\frac{1}{2}} \end{aligned} \tag{25}$$

$$U_{CAF,\text{identified}} = \pm(B^2_{CAF,\text{identified}} + P^2_{CAF})^{\frac{1}{2}} \tag{26}$$

$$\begin{aligned} B_{CN,\text{identified}} = \pm\Bigg(&\left[\frac{\partial CN}{\partial p0}B_{p0}\right]^2 + \left[\frac{\partial CN}{\partial pw}B_{pw}\right]^2 \\ &+ \left[\frac{\partial CN}{\partial DM}(k\cdot B_{DM})\right]^2 + \left[\frac{\partial CN}{\partial FN_M}B_{FN_M}\right]^2 + \left[\frac{\partial CN}{\partial FN_W}B_{FN_W}\right]^2 \\ &+ 2\frac{\partial CN}{\partial p0}\frac{\partial CN}{\partial pw}B'_{p0}B'_{pw} + 2\frac{\partial CN}{\partial FN_M}\frac{\partial CN}{\partial FN_W}B'_{FN_M}B'_{FN_W}\Bigg)^{\frac{1}{2}} \end{aligned} \tag{27}$$

$$U_{CN,\text{identified}} = \pm(B^2_{CN,\text{identified}} + P^2_{CN})^{\frac{1}{2}} \tag{28}$$

$$\begin{aligned} B_{CM,\text{identified}} = \pm\Bigg(&\left[\frac{\partial CM}{\partial p0}B_{p0}\right]^2 + \left[\frac{\partial CM}{\partial pw}B_{pw}\right]^2 \\ &+ \left[\frac{\partial CM}{\partial DM}(m\cdot B_{DM})\right]^2 + \left[\frac{\partial CM}{\partial My_M}B_{My_M}\right]^2 + \left[\frac{\partial CM}{\partial My_W}B_{My_W}\right]^2 \\ &+ 2\frac{\partial CM}{\partial p0}\frac{\partial CM}{\partial pw}B'_{p0}B'_{pw} + 2\frac{\partial CM}{\partial My_M}\frac{\partial CM}{\partial My_W}B'_{My_M}B'_{My_W}\Bigg)^{\frac{1}{2}} \end{aligned} \tag{29}$$

$$U_{CM,\text{identified}} = \pm(B^2_{CM,\text{identified}} + P^2_{CM})^{\frac{1}{2}} \tag{30}$$

IV. Results and Discussions

A. Axial Force

Uncertainty identification results for axial force at a Mach number of 2.0 are shown in Fig. 15. At angles of attack of 0, −6, +3, and +6°, the assessed uncertainties of the $D = 45$ model by the streamwise position test agreed with those by the vertical position test.

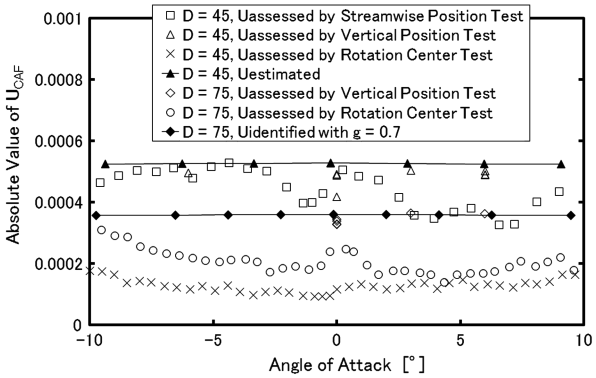

Fig. 15 Uncertainty identification results for axial force.

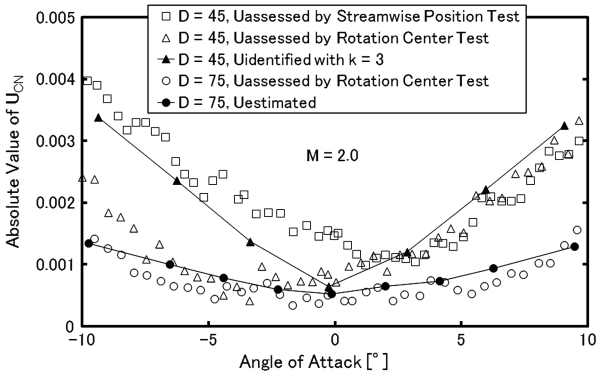

Fig. 16 Uncertainty identification results for normal force.

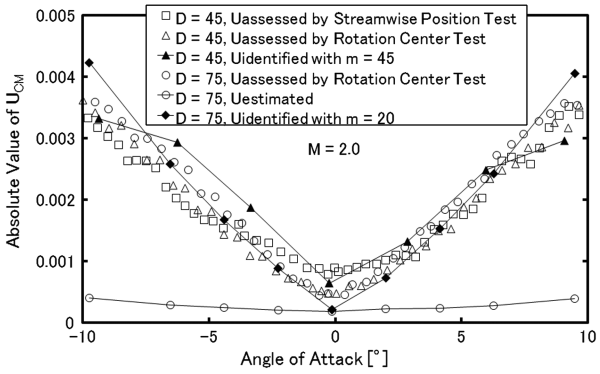

Fig. 17 Uncertainty identification results for pitching moment.

The experimentally assessed uncertainties of both models by the rotation center tests were smaller than those by the vertical position test, particularly at a small angle of attack. This is because the offset distances from the symmetric plane of the nozzle are considered to be insufficient in the rotation center test. Accordingly, at small angles of attack, the models might be exposed to the smaller nonuniformities than required.

From a conservative point of view, the assessed uncertainties by the vertical position tests were chosen as the equivalent uncertainties. For the $D = 45$ model, the initially estimated uncertainties agreed with the equivalent uncertainties. For the $D = 75$ model, the correction factor was calculated as $g = 0.7$ and the identified uncertainties agreed with the equivalent uncertainties at angles of attack of 0, $+3$, and $+6°$. This value is probably due to the large model size; the large model averages the nonuniformity error.

B. Normal Force

Uncertainty identification results for normal force at a Mach number of 2.0 are shown in Fig. 16. At positive angles of attack, the assessed uncertainties of the $D = 45$ model by the rotation center test agreed with those by the streamwise position test; however, at negative angles of attack, the assessed uncertainties by the former test were smaller than those by the latter test.

The estimated uncertainty for the $D = 45$ model did not agree with the assessed uncertainties of the $D = 45$ model. Then, the correction factor k for DM was calculated as three so that the identified uncertainties would agree the maximum assessed uncertainties at all angles of attack.

The simplest correction factor effectively identified the uncertainties at various angles of attack. If necessary, we can use more complex functions of angle of attack.

C. Pitching Moment

Uncertainty identification results for pitching moment at a Mach number of 2.0 are shown in Fig. 17. The assessed uncertainties of the $D = 45$ model by the streamwise position test agreed well with those by the rotation center test. The assessed uncertainties of the $D = 75$ model by the rotation center test showed reasonable agreement with those of the $D = 45$ model by both the streamwise position test and the rotation center test. Because the estimated uncertainties for both models were smaller than these assessed uncertainties, the correction factors were calculated as 45 and 20 for the $D = 45$ and $D = 75$ models, respectively. In this case as well, the simplest correction factors identified the uncertainties at various angles of attack.

D. Correction Factors Under Various Conditions

The identified correction factors for the two models at four Mach numbers are shown in Table 1. As shown in the table, the correction factors are dependent on the Mach number and the largest correction factor for the $D = 75$ model is 120 at a Mach number of 1.4. This correction factor corresponds to a dynamic pressure error of 2% because of the sensitivity of the Mach number to dynamic pressure.

The correction factors of the rotation center tests for CN and CM and those of the vertical position tests for CAF showed reasonable agreement with the corresponding results of the streamwise position tests. In the streamwise position test, the model is exposed to all the flow quality errors on the center line, but it is necessary to use the smaller model. However, the rotation center test and the vertical position test can be conducted with any models of interest. Additionally, these correction factors also depend on the model size. If the model is as large as the $D = 75$ model, whose length is 638 mm, it is not possible to conduct the streamwise position test. It is somewhat difficult to identify the correction factor for CAF by the rotation center tests, because the model is exposed to the stream nonuniformities smaller than required especially at small angles of attack.

The correction factors of the rotation center tests for CN and CM and those of the vertical position tests for CAF were selected to combine the uncertainty of the aerodynamic coefficients in the stability axes. These correction factors include the effects of the model area distribution and the moment arm on the model. They also include the data variations caused by the dynamic component of the flow quality during the eight tests. Consequently, the uncertainty caused by flow quality was adequately modeled by the correction factor about the model of interest. The uncertainties of lateral force and moments can be identified in the same way because the flow

Table 1 Correction factors for two models at four Mach numbers

Model		$D = 45$ AGARD-B ($L = 383$)				$D = 75$ AGARD-B ($L = 638$)			
Mach number	——	1.4	1.6	2.0	3.0	1.4	1.6	2.0	3.0
Mach angle, °	——	45.5	38.7	30	19.5	45.5	38.7	30	19.5
B_{DM}	——	0.009	0.009	0.006	0.009	0.009	0.009	0.006	0.009
g for CAF	Streamwise position test	0.8	1.5	1	0.8	——	——	——	——
	Vertical position test	0.6	1	1	0.8	0.5	0.6	0.7	0.5
	Rotation center test	0.2	0.2	0.2	0.2	0.2	0.2	0.4	0.2
k for CN	Streamwise position test	25	5	3	1	——	——	——	——
	Rotation center test	25	4	3	1	25	3	1	1
m for CM	Streamwise position test	200	36	45	25	——	——	——	——
	Rotation center test	135	20	45	25	120	30	20	3.5

quality errors contribute to them through the same mechanism as longitudinal forces and moment. The uncertainty of supersonic wind-tunnel testing is almost dominated by characterization of the tunnel flow quality.

E. Practically Independent Parameters

For longitudinal forces and moment, the coefficients in the stability axes are usually used for the development of aircraft, whereas those in the body axes are actually measured around an internal balance center. It is necessary to obtain not only the data but also the uncertainty in both the axes. Moreover, the error of each component of the actually measured coefficient in the body axes is supposed to have each practically independent uncertainty, because the uncertainties of these coefficients are independently dominated by characterization of the flow quality, as shown in the previous discussions.

Because of this independence, uncertainties of the stability axes coefficients can be combined with the identified uncertainties of the body axes coefficients as shown in the following equations. Therefore, uncertainties of any kind of coefficients, such as derivatives of sideslip angles, can be combined with those of the body axes coefficients. This procedure drastically reduces the calculation complexity because the AIAA standard recommends the calculation of the uncertainty of all the results from the actually measured variables and constants as shown in Eqs. (8–21). In the following equations, the uncertainties of the stability axes coefficients are expressed as functions of the bias and precision limits both of the body axes coefficients and others

$$CLF = CN\cos\alpha - CAF\sin\alpha \tag{31}$$

$$B_{CLF,\text{combined}} = \pm\left(\left[\frac{\partial CLF}{\partial CN}B_{CN,\text{identified}}\right]^2 + \left[\frac{\partial CLF}{\partial CAF}B_{CAF,\text{identified}}\right]^2 + \left[\frac{\partial CLF}{\partial\theta}B_\theta\right]^2 + \left[\frac{\partial CLF}{\partial\phi}B_\phi\right]^2\right)^{\frac{1}{2}} \tag{32}$$

$$P_{CLF,\text{combined}} = \pm\left(\left[\frac{\partial CLF}{\partial CN}P_{CN}\right]^2 + \left[\frac{\partial CLF}{\partial CAF}P_{CAF}\right]^2 + \left[\frac{\partial CLF}{\partial\theta}P_\theta\right]^2 + \left[\frac{\partial CLF}{\partial\phi}P_\phi\right]^2\right)^{\frac{1}{2}} \tag{33}$$

$$U_{CLF,\text{combined}} = \pm(B^2_{CLF,\text{combined}} + P^2_{CLF,\text{combined}})^{\frac{1}{2}} \tag{34}$$

$$CDF = CAF\cos\alpha + CN\sin\alpha \tag{35}$$

$$B_{CDF,\text{combined}} = \pm\left(\left[\frac{\partial CDF}{\partial CAF}B_{CAF,\text{identified}}\right]^2 + \left[\frac{\partial CDF}{\partial CN}B_{CN,\text{identified}}\right]^2 + \left[\frac{\partial CDF}{\partial\theta}B_\theta\right]^2 + \left[\frac{\partial CDF}{\partial\phi}B_\phi\right]^2\right)^{\frac{1}{2}} \tag{36}$$

$$P_{CDF,\text{combined}} = \pm\left(\left[\frac{\partial CDF}{\partial CN}P_{CN}\right]^2 + \left[\frac{\partial CDF}{\partial CAF}P_{CAF}\right]^2 + \left[\frac{\partial CDF}{\partial\theta}P_\theta\right]^2 + \left[\frac{\partial CDF}{\partial\phi}P_\phi\right]^2\right)^{\frac{1}{2}} \tag{37}$$

$$U_{CDF,\text{combined}} = \pm(B^2_{CDF,\text{combined}} + P^2_{CDF,\text{combined}})^{\frac{1}{2}} \tag{38}$$

$$Cm = CM - \frac{CN\cdot(X_B - X_C)}{c} + \frac{CAF\cdot(Z_B - Z_C)}{c} \tag{39}$$

$$B_{Cm,\text{combined}} = \pm\left(\left[\frac{\partial Cm}{\partial CM}B_{CM,\text{identified}}\right]^2 + \left[\frac{\partial Cm}{\partial CN}B_{CN,\text{identified}}\right]^2 + \left[\frac{\partial Cm}{\partial CAF}B_{CAF,\text{identified}}\right]^2 + \left[\frac{\partial Cm}{\partial X_B}B_{X_B}\right]^2 + \left[\frac{\partial Cm}{\partial X_C}B_{X_C}\right]^2 + \left[\frac{\partial Cm}{\partial Z_B}B_{Z_B}\right]^2 + \left[\frac{\partial Cm}{\partial Z_C}B_{Z_C}\right]^2 + 2\frac{\partial Cm}{\partial X_B}B'_{X_B}\frac{\partial Cm}{\partial X_C}B'_{X_C} + 2\frac{\partial Cm}{\partial Z_B}B'_{Z_B}\frac{\partial Cm}{\partial Z_C}B'_{Z_C}\right)^{\frac{1}{2}} \tag{40}$$

$$P_{Cm,\text{combined}} = \pm\left(\left[\frac{\partial Cm}{\partial CM}P_{CM}\right]^2 + \left[\frac{\partial Cm}{\partial CN}P_{CN}\right]^2 + \left[\frac{\partial Cm}{\partial CAF}P_{CAF}\right]^2 + \left[\frac{\partial Cm}{\partial X_B}P_{X_B}\right]^2 + \left[\frac{\partial Cm}{\partial X_C}P_{X_C}\right]^2 + \left[\frac{\partial Cm}{\partial Z_B}P_{Z_B}\right]^2 + \left[\frac{\partial Cm}{\partial Z_C}P_{Z_C}\right]^2\right)^{\frac{1}{2}} \tag{41}$$

$$U_{Cm,\text{combined}} = \pm(B^2_{Cm,\text{combined}} + P^2_{Cm,\text{combined}})^{\frac{1}{2}} \tag{42}$$

F. Validation of Combined Uncertainties

These combined uncertainties were validated in correlation results of the tunnel-to-tunnel comparison tests. If another wind tunnel has the equivalent flow quality to that of the JSWT, it is anticipated that the data of the same model configuration obtained in this wind tunnel have the same amounts of uncertainty interval. Accordingly, the data scatters around the true value can be explained by the JSWT uncertainties. On the other hand, the differences from the data of the JSWT to the data obtained in another wind tunnel with the larger error contributions of flow quality could not be explained by the JSWT uncertainties.

Table 2 shows wind tunnels, diameter D of the AGARD-B models and Reynolds number based on the model length ReL at a Mach number of 2.0 in the comparison tests. All the tests were conducted with state-of-the-art instrumentation and balances to keep the uncertainty an absolute minimum.

The common $D = 75$ model with the same balance, sting, roughness and pressure transducers was tested both in the JSWT (JAXA 1 m × 1 m supersonic wind tunnel) and in the DTWT (2 m × 2 m blowdown-type trisonic wind tunnel) [23], the latter tunnel is operated by the TRDI (Technical Research and

Table 2 Wind tunnels and test conditions of tunnel-to-tunnel comparison tests at a Mach number of 2.0

Case No.	Organization	Test section	Tunnel	Model Dia. D [mm]	ReL [$\times 10^6$]	Remarks
#1	JAXA	1 m × 1 m	JSWT	45	10.7	In Sept. 2008
#2				75	17.9	In April 2008
#3				75	17.9	In Oct. 2008
#4				75	17.9	In Oct. 2008 at roll angle of 180°
#5	TRDI	2 m × 2 m	DTWT	75	19.7	In Jan. 2008
#6				150	37.7	In 2003
#7	ONERA	1.93 m × 1.75 m	S2MA	150	24.2	In 2003 with a 2-D asymmetric nozzle

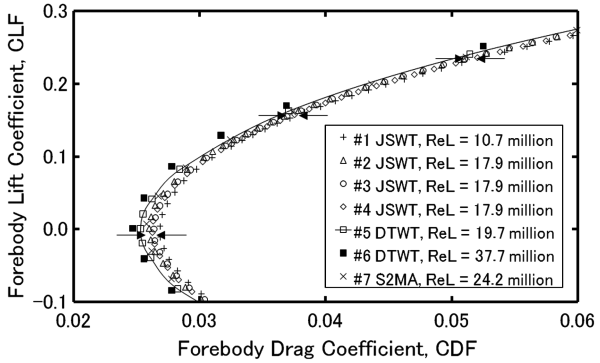

Fig. 18 Correlation result of drag coefficients obtained in three wind tunnels.

Development Institute) of the Ministry of Defense, Japan. The DTWT was constructed by the same manufacturer of the JSWT and the nozzle aerolines were optimized by the same methodology as those of the JSWT. Thus, the DTWT has almost the same uniformities of freestream Mach number as shown in Fig. 3 [24]. Another comparison test was conducted with another common AGARD-B model with a reference diameter of 0.15 m in the DTWT and in the ONERA S2MA continuous wind tunnel in France [24].

The correlation results of forebody drag, lift force, and pitching moment at a Mach number of 2.0 are shown in Fig. 18 and 19. A total of seven test results are plotted; the combined uncertainties for the JSWT data of the $D = 75$ model are shown as two-headed arrows. The uncertainties of the lift force coefficients are so small that they are identical to the mark width. Three tests were performed in the JSWT in a period of six months or at roll angle of 180°.

As Reynolds number increased, the drag coefficients decreased because of the Reynolds number effect [11]. However, it was found that small differences of Reynolds number around 20 million based on the model length are negligible to discuss the uncertainty intervals. The data obtained at the Reynolds number around 20 millions fell almost within the uncertainty intervals of the JSWT data for the $D = 75$ model, although the DTWT data showed larger differences than the uncertainty intervals around the JSWT data. However, if the DTWT data have the same amounts of the uncertainty intervals as those of the JSWT, we can find sufficient overlapping portions of both the uncertainty intervals between the data of the DTWT and the data of the JSWT. The differences between the JSWT data and the DTWT data correspond approximately to the combined uncertainty intervals. It suggests us all the error source are appropriately assessed [19].

The pitching moment data of the different size models, or in the different wind tunnels show some scatters because they have the different errors caused by the flow qualities. However, except the S2MA data, all the pitching moment data fell within the uncertainty intervals of the JSWT data for the $D = 75$ model. The S2MA data show larger differences than the uncertainty intervals. It is probably

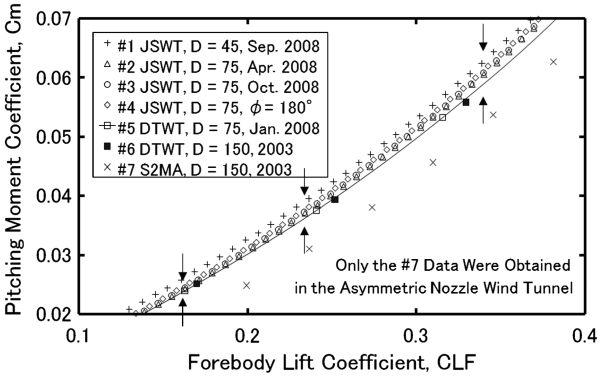

Fig. 19 Correlation result of pitching moment coefficient obtained in three wind tunnels.

because the S2MA uses the 2-D asymmetric supersonic nozzle whereas the others use the 2-D symmetric nozzle. The asymmetric nozzle produces asymmetric flows as the model experience at the offset position from the center line of the symmetric nozzle. Such an asymmetric nozzle flow might cause the larger error contributions to the longitudinal force and moment. If the multiposition tests proposed in this paper is conducted in the asymmetric nozzle wind tunnel, another amount of the uncertainty interval would be found.

Consequently, the differences between the various data are successfully explained by the combined uncertainties. Thus, the uncertainties estimated by the methodology proposed in this paper are validated.

V. Conclusions

In this study, a methodology to estimate the uncertainty of supersonic wind-tunnel testing has been developed. In addition to stream nonuniformities, the asymmetric flowfield at the offset position from the symmetric plane of the 2-D nozzle also contributes considerably to the uncertainties of aerodynamic force and moment. Further, uncertainties of aerodynamic coefficients in body axes are well identified from the test data with changing rotation centers and vertical positions, which can be performed with any models of interest. The uncertainties of all components of the aerodynamic coefficients in the body axes are almost dominated by characterization of flow quality and found to be practically independent of each other. Thus, the uncertainties of aerodynamic coefficients in stability axes are successfully estimated by combining the identified uncertainties of the body axes coefficients. As a result, in the case of supersonic flow, it is possible to estimate the uncertainty of wind-tunnel testing without time-consuming multifacility wind-tunnel testing.

Acknowledgments

The authors thank Y. Itabashi, H. Nishijima, T. Kimura, J. Akatsuka, H. Kanda, M. Sato, and M. Watanabe for supporting our wind-tunnel testing.

References

[1] "Assessment of Experimental Uncertainty with Application to Wind Tunnel Testing," AIAA S-071A-1999, Reston, VA, 1999.

[2] Arrington, J. P., and Jones, J. J. (ed.), "Shuttle Performance: Lesson Learned," NASA CP2283 part 1, 1983.

[3] RTO Applied Vehicle Technology Panel (AVT) (ed.), "A Feasibility Study of Collaborative Multi-facility Windtunnel Testing for CFD Validation," RTO-TR-27, The Research and Technology Organization (RTO) of NATO, 1999.

[4] Mejia, K. M., "A Comprehensive Review of High Speed Wind Tunnel Performance Data from the Boeing High Speed Civil Transport Program," AIAA Paper 2001-0453, 2001.

[5] Belter, D. L., "Comparison of Wind Tunnel Data Repeatability with Uncertainty Analysis Estimates," AIAA Paper 98-2714, 1998.

[6] Cahill, D. M., "Application of Uncertainty Methodology for the Wind Tunnel Facilities at AEDC," AIAA Paper 96-2216, 1996.

[7] Springer, A. M., "Uncertainty Analysis of the NASA MSFC 14-inch Trisonic Wind Tunnel," AIAA Paper 99-0684, 1999.

[8] Kammeyer, M. E., "Wind Tunnel Facility Calibrations and Experimental Uncertainty," AIAA Paper 98-2715, 1998.

[9] Aeschliman, D. P., and Oberkampf, W. L., "Experimental Methodology for Computational Fluid Dynamics Code Validation," *AIAA Journal*, Vol. 36, No. 5, 1998, pp. 733–741. doi:10.2514/2.461

[10] Nagai, S., Tsuda, S., Koyama, T., Hirabayashi, N., and Sekine, H., "Validity of Statistical Uncertainty in Comparison of Winged Vehicle Force Data at Hypersonic Wind Tunnels," *Journal of the Japan Society for Aeronautical and Space Sciences*, Vol. 51, No. 591, 2003, pp. 151–157. doi:10.2322/jjsass.51.151

[11] Hills, R. (ed.), "A Review of Measurements on AGARD Calibration Models," AGARDograph 64, 1961, Part 3.

[12] Nomura, R., Kawamoto, H., Yoshida, H., Yoneda, T., and Aoki, S., "Geometry Optimization of Supersonic Wind Tunnel Nozzle (1st Report, Development of Optimization Method Focused on the Flow

Characteristics in the Nozzle)," *Transactions of the Japan Society of Mechanical Engineers, Series B*, Vol. 69, No. 680, 2003, pp. 854–860.

[13] Ames Research Staff, Equations, Tables, and Charts for Compressible flow, NACA TR-1135, 1953, pp. 619.

[14] AIAA (ed.), Assessment of Experimental Uncertainty with Application to Wind-Tunnel Testing, AIAA Paper S-071A-1999, Reston, VA, 1999, Chap. 2.

[15] Nagai, S., Iijima, H., Kanda, H., Watanabe, M., and Sato, M., "Uncertainties of Aerodynamic Coefficients at a Supersonic Wind Tunnel," *Journal of the Japan Society for Aeronautical and Space Sciences*, Vol. 54, No. 634, 2006, pp. 485–491. doi:10.2322/jjsass.54.485

[16] AGARD's Fluid Dynamics Panel (ed.), "A Selection of Experimental Test Cases for the Validation of CFD Codes," AGARD AR-303, 1994, Chap. 3.

[17] AIAA (ed.), "Assessment of Experimental Uncertainty with Application to Wind Tunnel Testing," AIAA Paper S-071A-1999, Reston, VA, 1999, Annex 2-A.

[18] Young, J. C., and Underwood, J. M., "The Development of Aerodynamic Uncertainties for the Space Shuttle Orbiter," AIAA Paper 82-0563, 1982.

[19] ASME (ed.), "ASME Performance Test Codes, Supplement on Instruments and Apparatus. Part 1: Measurement Uncertainty," Rept. No.ANSI/ASME PTC19.1, Japan Society of Mechanical Engineering, Tokyo, 1987, Chap. 3 (translated by Japan Society of Mechanical Engineers).

[20] Anderson, J. D., Jr., *Fundamentals of Aerodynamics*, McGraw–Hill, New York, 1982, Chap. 13.

[21] Pope, A., and Goin, K. L., *High-Speed Wind Tunnel Testing*, Wiley, New York, 1965, p. 359.

[22] AIAA (ed.), Assessing Experimental Uncertainty-Supplement to AIAA S-071A-1999; also AIAA G-045-2003, Reston, VA, 2003, Chap. 7.

[23] Takao, S., Ono, H., Udagawa, T., Iijima, H., and Nagai, S., "The Correlation Wind Tunnel Testing in TWT and SWT1," *Proceedings of the 46th Aircraft Symposium* [CD-ROM], 2008, pp. 612–618.

[24] Ono, H., Ebina, T., Noto, K., Yoneda, T., Kawamura, T., Nagaya, H., and Kimura, N., "Flow Quality Measurement in the MOD Trisonic Wind Tunnel: Supersonic Speed Range," *Proceedings of the 45th Aircraft Symposium* [CD-ROM], 2007, pp. 842–850.